An Improved Land Surface Emissivity Parameter for Land Surface Models Using Global Remote Sensing Observations

Menglin Jin

Department of Atmospheric and Oceanic Science, University of Maryland, College Park, College Park, Maryland

Shunlin Liang

Department of Geography, University of Maryland, College Park, College Park, Maryland

ABSTRACT

Because land surface emissivity (ε) has not been reliably measured, global climate model (GCM) land surface schemes conventionally set this parameter as simply constant, for example, 1 as in the National Oceanic and Atmospheric Administration (NOAA) National Centers for Environmental Prediction (NCEP) model, and 0.96 for bare soil as in the National Center for Atmospheric Research (NCAR) Community Land Model version 2 (CLM2). This is the so-called constant-emissivity assumption. Accurate broadband emissivity data are needed as model inputs to better simulate the land surface climate. It is demonstrated in this paper that the assumption of the constant emissivity induces errors in modeling the surface energy budget, especially over large arid and semiarid areas where ε is far smaller than unity. One feasible solution to this problem is to apply the satellite-based broadband emissivity into land surface models.

The Moderate Resolution Imaging Spectroradiometer (MODIS) instrument has routinely measured spectral emissivities (ε_λ) in six thermal infrared bands. The empirical regression equations have been developed in this study to convert these spectral emissivities to broadband emissivity (ε) required by land surface models. The observed emissivity data show strong seasonality and land-cover dependence. Specifically, emissivity depends on surface-cover type, soil moisture content, soil organic composition, vegetation density, and structure. For example, broadband ε is usually around 0.96–0.98 for densely vegetated areas [(leaf area index) LAI > 2], but it can be lower than 0.90 for bare soils (e.g., desert). To examine the impact of variable surface broadband emissivity, sensitivity studies were conducted using offline CLM2 and coupled NCAR Community Atmosphere Models, CAM2–CLM2. These sensitivity studies illustrate that large impacts of surface ε occur over deserts, with changes up to $1°–2°C$ in ground temperature, surface skin temperature, and 2-m surface air temperature, as well as evident changes in sensible and latent heat fluxes.

1. Introduction

Emissivity (ε) is the ratio of energy emitted from a natural material to that from an ideal blackbody at the same temperature. Accurate surface ε is desired in land surface models for better simulations of surface energy budgets from which skin temperature in the model is calculated (Jin et al. 1997). Lacking global ε observations, the first comprehensive land surface models coupled to global climate models (GCMs) simply assumed ε to be 1 (Dickinson et al. 1986; Sellers et al.

1986). Later many land surface models adopted this assumption by setting ε as 1 or constants close to 1. Although the constant-ε[1] assumption provides first-order approximation, it induces errors in simulating surface-upward longwave radiation, and, consequently, radiative energy redistribution. Although constant-ε assumption may be valid for most vegetated areas where ε is close to unity, it is not true for arid and semiarid areas. For example, $\varepsilon = 0.7–0.8$ were observed over the Saharan deserts at 9 μm due to large quartz levels there (Rowntree 1991; Prabhakara and Dalu 1976), and thus

---

Corresponding author address: Dr. Menglin Jin, Department of Atmospheric and Oceanic Science, University of Maryland, College Park, College Park, MD 20772.
E-mail: mjin@atmos.umd.edu

---

[1] Here the "constant-ε" assumption indicates a twofold problem. First, ε is assumed to be constant when it actually varies in space and time. Second, ε is assumed to be near 1, which is incorrect for certain surfaces.
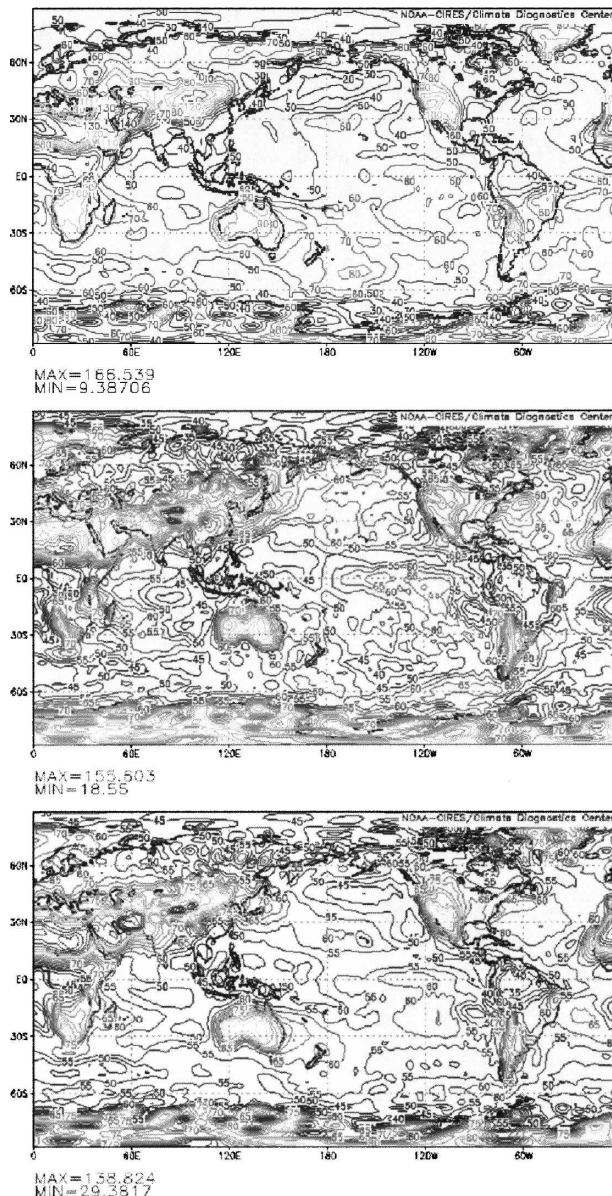
FIG. 1. (a) NCEP–NCAR reanalysis for July 2001, surface net longwave radiation. (b) Same as in (a), but for November 2001. (c) Same as (a), but for the annual mean for 2001.

assuming $\varepsilon = 1$ may result in an error of about 15 W m^{-2} in the net longwave radiation annually given the fact that the desert surface emissivity is 0.90 in many areas from the Moderate Resolution Imaging Spectroradiometer (MODIS) observations and the annual net longwave radiation is about 160 W m^{-2} [see Fig. 1 and Eq. (8)]. The instantaneous error may be higher when the surface net radiation is above the annual mean.

In the land surface model of the National Center for Atmospheric Research (NCAR), the Community Land Model version 2 (CLM2), there are three surface emis-

sivities: bare soil emissivity, canopy emissivity (ε_c), and snow emissivity. Except that ε_c is calculated very simply as a function of leaf area index (LAI), the other emissivity values are prescribed as 0.96 for soil and 0.97 for snow, respectively. Therefore, emissivity treatment is still a problem in CLM2 when soil emissivity is set as constant since this variable can shift more than 10% around the globe from the MODIS observations we present below.

The goal of this work is to examine whether the constant-ε assumption currently used in land surface models is realistic, and to study the impact of ε on land surface modeling. To achieve that, we employed two methods. First, the emissivity products from MODIS were analyzed to demonstrate the global distribution, seasonal variation, and ε–LAI relationship. Second, the NCAR offline CLM2 and NCAR Community Atmosphere Model (CAM) coupled with CLM2 (CAM–CLM2) were used to conduct a series of sensitivity studies.

Remotely sensing surface ε is very challenging because of the high heterogeneity of land surfaces and the difficulties in removing atmospheric effects (Wan and Li 1997; Liang 2001, 2004). Furthermore, there is a mismatch between what remote sensing provides and what land surface models need: remote sensing measures spectral emissivity (ε_λ) through channels at certain wavelengths (λ) but land surface models need "broadband" emissivity for calculating upward longwave radiation using the Stefan–Boltzmann law. Due to atmospheric absorption, only the spectral radiance within the infrared water vapor window region (i.e., 8–14 μm) is measured by thermal infrared remote sensing. It is these measurements that need to be converted into broadband emissivity. In this study, a regression equation based on radiative transfer model is derived to convert MODIS spectral emissivities into broadband emissivity. More details are available in section 2c.

In the remaining part of this paper, section 2 describes the properties of emissivity and its role in land surface equations. Section 3 introduces the observations and the models used in this work. Sections 4 and 5 present results, discussions, and conclusions.

2. Background

a. Properties of emissivity

Conceptually, all materials are formed by molecules with atoms bonded together inside through molecular bonds. Atoms vibrate at the end of a bond when agitated by light of particular wavelength hitting the molecule. In turn, the molecule reemits the same wavelength of light. This is the "absorption and emission"

process. Only light in the infrared spectrum causes molecular vibration. Since every unique molecule has its own characteristic frequency of vibration, a natural surface that emits infrared light depends on surface composition; therefore, the emissivity spectrum is distinct depending on surface composition. Simply put, if the surface is of mixed types, its emissivity is different from the surface types that it was composed of.

Emissivity is defined as

$$\varepsilon_\lambda = E_\lambda / B_\lambda(T), \tag{1}$$

where E_λ is the emitted radiance at wavelength λ and $B_\lambda(T)$ is the blackbody emission at wavelength λ and temperature T, which can be calculated from the Planck function.

Kirchoff's law states that the emissivity of an opaque body at thermodynamic equilibrium is equal to absorptivity, and therefore based on the conservation of energy, the reflectivity R_λ and emissivity is

$$R_\lambda = 1 - \varepsilon_\lambda. \tag{2}$$

It is difficult to determine the emissivity of an object for at least three reasons: emissivity is a surface property, and the surface of an object may change with time; the land surface is composed of various objects with different emissivities; and emissivity retrieval from remote sensing depends on the surface temperature, but accurate surface temperature is difficult to measure.

1) EMISSIVITY OF BARE SOIL

The emissivity of natural land surface is determined by soil structure, soil composition, organic matter, moisture content, and vegetation-cover characteristics (Van De Griend and Owe 1993), but does not depend on soil temperature profile or surface temperature. For bare soil, the key parameters affecting emissivity are the surface finish, the chemical composition, the soil's thermal and mechanical history, and the wavelength at which the emissivity is measured (Van De Griend and Owe 1993). Physically, emissivity is independent of bare soil temperature, but since thermal infrared radiance measured by satellite radiometer includes signals of both temperature and emissivity, emissivity has to be separated from temperature (Snyder et al. 1998).

Emissivity is determined partially by grain sizes of soil and organic content. Nerry et al. (1990) reported that the smaller the diameter of soil grain, the higher the emissivity over 10–14 μm from a sample of silicon carbide (SiC) sands (see their Fig. 7). The decrease of spectral contrast with decreasing grain-size diameter is a well-known effect (Logan et al. 1974) in a region where surface scattering dominates.

Land surface models require emissivity integrated over the longwave water vapor window region of

TABLE 1. Emissivity table of some common materials. This is not a comprehensive list and should be taken as a reference only. (Data taken from http://www.electro-optical.com/.)

Material	ε
Aluminum foil	0.04
Asbestos board	0.96
Asbestos paper	0.93
Asphalt (paving)	0.97
Brass (hard rolled—polished with lines)	0.04
(somewhat attacked)	0.04
Brick (red—rough)	0.93
Brick (silica—unglazed rough)	0.80
Carbon (T—carbon 0.9% ash)	0.81
Concrete	0.94
Copper (plate heavily oxidized)	0.78
Frozen soil	0.93
Glass (smooth)	0.94
Gold (pure highly polished)	0.02
Granite (polished)	0.85
Ice	0.97
Marble (light gray polished)	0.93
Paper (black tar)	0.93
Paper (white)	0.95
Plaster (white)	0.91
Plywood	0.96
Tin (bright tinned iron sheet)	0.04
Water	0.95
Wood (freshly planned)	0.90

8–14 μm. Therefore, for the purpose of understanding the impact of emissivity on model predictions, our study focuses only on this spectral region. Table 1 presents reference values of emissivity for some materials. It shows that emissivity varies significantly with chemical materials; therefore, the soil emissivity of a given sample is sensitive to its chemical compositions. Furthermore, environmental effects over the history of these chemical components may cause changes in properties (e.g., surface roughness or surface contamination) that affect emissivity (Francois et al. 1997).

2) EMISSIVITY OF THE CANOPY

Emissivity of the canopy, ε_c, is even more complex than the underlying soil emissivity. Single-leaf emissivity differs from that of integrated effective canopy emissivity (Fuchs and Tanner 1966; Van De Griend and Owe 1993; Francois et al. 1997), because ε_c is determined by the overall structure of the vegetation instead of the flat surface of leaves (i.e., the "cavity effect"). Cavity effects make ε_c larger than the single leaf's ε due to multiple internal reflections resulting from canopy geometry structure. For example, ε is from 0.95 to 0.98 for single leaves but is expected to increase for dense canopy (Fuchs and Tanner 1966). Idso et al. (1969) reported a leaf emissivity as low as 0.938. It was found

that the cavity effect becomes significant when the leaves' proportion exceeds the soil proportion (viz. about leaf area index LAI > 2). In addition, although different leaves show similar spectral reflectances in both visible and near-infrared wavelengths, distinct features of emissivity are noticed in the thermal-infrared region.

The plant species, vegetation density, and growth state all affect ε_c. Using a radiative transfer model, Francois et al. (1997) reported that as canopy LAI (i.e., the variable representing the greenness and density of vegetation from remote sensing) increases, the ε_c increases to a limit. Their model finds that the LAI profile, namely, vegetation vertical structure, has little effect on ε. The view angle modifies ε_c only for off-zenith angles greater than 50°.

A good review of ε and vegetation index was provided by Van De Griend and Owe (1993). Measured over a savanna environment, they found that thermal emissivity was highly positively correlated with the Normalized Difference Vegetation Index (NDVI) with a correlation coefficient as high as 0.94. Their field experiments measured $\varepsilon = 0.914$ for bare soil of loamy sand (NDVI = 0.157), 0.949 for partly covered open grass (NDVI = 0.278), 0.958 for long grass (NDVI = 0.276), 0.952 for partly covered shrub (NDVI = 0.367), and 0.986 for completely covered shrub (NDVI = 0.727). Following these measurements, they developed one logarithmic equation to describe the empirical relations between ε and NDVI. Note that their results were based on field experiments and only for the savanna; the application of their values in land surface model needs further verification for other vegetation types.

There are other factors affecting ε_c. Dynamic states of vegetation such as growing crops and idle crops (bare soil) have distinct ε (Snyder et al. 1998). In addition, water stress, for example, could also have some effect on the canopy emissivity (Francois et al. 1997).

b. Emissivity in the land surface model

The exchanges of momentum, heat, and moisture at the land surface in an atmosphere–vegetation–soil system are the key physical processes that determine the land surface thermodynamics and dynamics. The unique role of ε can be demonstrated in the energy balance equation that governs the heat and water exchanges:

$$R_n = \text{SH} + \text{LE} + G, \tag{3}$$

$$R_n = S_\downarrow - S_\uparrow + \text{LW}_\downarrow - \text{LW}_\uparrow, \tag{4}$$

$$\text{LW}_\uparrow = \varepsilon \sigma T_s^4, \tag{5}$$

where SH is the sensible heat flux, LE is the latent heat flux, and G is the ground heat flux. These three processes compete for surface net radiation R_n, which is the downward minus upward shortwave and longwave radiation. In Eq. (4), $S_\downarrow$ is the downward solar radiation, $S_\uparrow$ is the reflected solar radiation, $\text{LW}_\downarrow$ is the downward longwave radiation, and $\text{LW}\uparrow$ is the upward longwave radiation from the surface. Emissivity and surface skin temperature (T_s) determine the upward longwave radiation, or surface emission, following the Stefan–Boltzmann law.

We first theoretically analyze the possible ε effect. To keep the discussion simple, here we only analyze the case when $\varepsilon = 1$, for it gives maximum errors. If ε is set to 1, net longwave radiation is

$$\text{LW}_n^{\varepsilon=1} = \text{LW}_\downarrow - \sigma T_s^4, \tag{6}$$

while, in fact, this term should be

$$\text{LW}_n^{\varepsilon \neq 1} = \text{LW}_\downarrow - \varepsilon \sigma T_s^4 - (1 - \varepsilon)\text{LW}_\downarrow. \tag{7}$$

Therefore, the error induced by the unit emissivity assumption is

$$\Delta = \text{LW}_n^{\varepsilon \neq 1} - \text{LW}_n^{\varepsilon=1}$$
$$= \underbrace{(\sigma T_s^4 - \text{LW}_\downarrow)}_{A}\underbrace{(1 - \varepsilon)}_{B}, \tag{8}$$

where Δ is the error in net longwave radiation if accurate ε is not taken into account in land surface models. Equation (8) implies two situations when large errors may occur due to inaccurate ε: where there are large differences between upward and downward longwave radiation (term A), and where the surface ε greatly departs from unity (term B).

We used the National Oceanic and Atmospheric Administration (NOAA) National Centers for Environmental Prediction (NCEP) reanalysis to examine when and where the first situations may occur. Figure 1 shows the magnitude of term A of Eq. (8) over the globe. These analyses were based on the NCEP reanalysis for July, November, and the annual mean for the year 2001, respectively. Large net longwave radiation centers are shown over desert areas including the Sahara, Australia, southwest North America, and the central desert areas of Eurasia. These deserts are associated by hot, downwelling branches of the Hadley circulation. With the displacement of general circulation in different seasons, the strength and locations of the net longwave radiation centers vary moderately from season to season. For example, the maximum for term A is in the Sahara in July but moves to Eurasia in November, with values of 166 and 155 W m^{-2}, respectively. Meanwhile, as bare soil with little moisture and vegetation, these areas have small ε values that are far from 1; therefore,
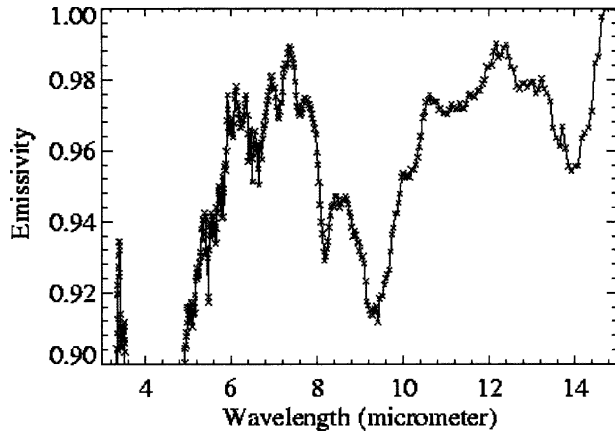
large Δ are expected to occur over these areas. The Sahara, for instance, may have annual mean Δ around 15 W m^{-2}, given a term A value of about 160 W m^{-2} and emissivity of 0.90 (see section 4). Instantaneously, the error may be due to a longer value of term A. This Δ will propagate an error in skin temperature and heat fluxes, as we prove later. For nondesert regions, where emissivity is higher and term A is smaller, the constant-emissivity assumption may be tolerable. We will use model sensitivity studies to examine this possible tolerance in section 3.

c. Broadband emissivity conversion

Remote sensing retrieves emissivity from individual spectral bands (i.e., ε_λ) while GCM's land surface model needs broadband emissivity (i.e., ε). Therefore, a conversion from narrowband into broadband is necessary. Outside of the water vapor window, LW$_\downarrow$ originates from the levels close to the ground and thus differs little from the surface emission. Consequently, only surface radiation at the window region is critical for the surface radiation budget (Rowntree 1991; R. E. Dickinson 2003, personal communication). In other words, only window region spectral emissivity needs to be taken into account during spectral–broadband emissivity conversion. Note that even in the water vapor window, the presence of clouds will increase the downwelling longwave above its clear-sky value, and thus reduce the Δ described in Eq. (8). Nevertheless, for desert and semidesert regions, the cloud effect is ignorable.

Figure 2 shows the variation of emissivity as a function of wavelength for soil. Evidently, for different samples of soil, ε_λ is different because of the differing chemical composition of the soils. The ε_λ varies from

0.91 at 9.1 μm to 0.98 at 14.5 μm. The spectral emissivity value in Fig. 2 beyond 14.5 μm is not reliable due to the strong atmospheric absorption. The large irregular variations with wavelength make it difficult to derive a broadband ε. In this work, we conducted extensive simulations incorporating thousands of surface emissivity spectra, and then derived the regression equations as the function of the MODIS spectral emissivity values. Broadband ε should be seen as a first-order approximation for capturing the integrated features of ε from MODIS spectral bands. Figure 3 gives an example of global broadband emissivities for January and July 2003, respectively. Emissivity depends on land cover, with high values over dense vegetation regions and apparently low values over desert regions. In addition, seasonality is evident over Sahara Desert edges and boreal forests in the Northern Hemisphere.

The procedure for developing conversion formulas of spectral emissivities to broadband emissivity consists of the following steps. First, thousands of measured emissivity spectra from different sources [e.g., Advanced Spaceborne Thermal Emission and Reflection Radiometer (ASTER) spectral library, Salisbury database, the U.S. Geological Survey spectral library] have been collected. Second, broadband "effective" emissivity is calculated using the Planck equation and spectral emissivity spectra. Third, integrating these surface spectral emissivity spectra with the sensor spectral response functions leads to the simulated MODIS spectral emissivities. Finally, a linear relationship is established between the broadband emissivity (ε) and MODIS spectral emissivities (ε_i) through regression analysis:

$$\varepsilon_{8-14} = 0.0139\varepsilon_{29} + 0.4606\varepsilon_{31} + 0.5256\varepsilon_{32}. \quad (10)$$

Although MODIS has four bands in 8–12 μm (bands 29–32[2]), not all of them are incorporated in the formula above because of their correlation and large uncertainties in estimating the spectral emissivity at band 30.

MODIS has two different algorithms for estimating spectral emissivities (Wan and Li 1997). One of them is based on land-cover information that may determine the spectral emissivity in bands 31 and 32 far more accurately than other bands. If only emissivities of bands 31 and 32 are used, the formula is

$$\varepsilon_{8-14} = 0.4587\varepsilon_{31} + 0.5414\varepsilon_{32}. \quad (11)$$

Nevertheless, the broadband emissivity estimated only from emissivities in MODIS bands 31 and 32 [Eq. (11)] may not be too accurate, because of lacking informa-

---

[2] Band 29 is 8.400–8.700 μm, band 31 is 10.780–11.280 μm, and band 32 is 11.770–12.270 μm.
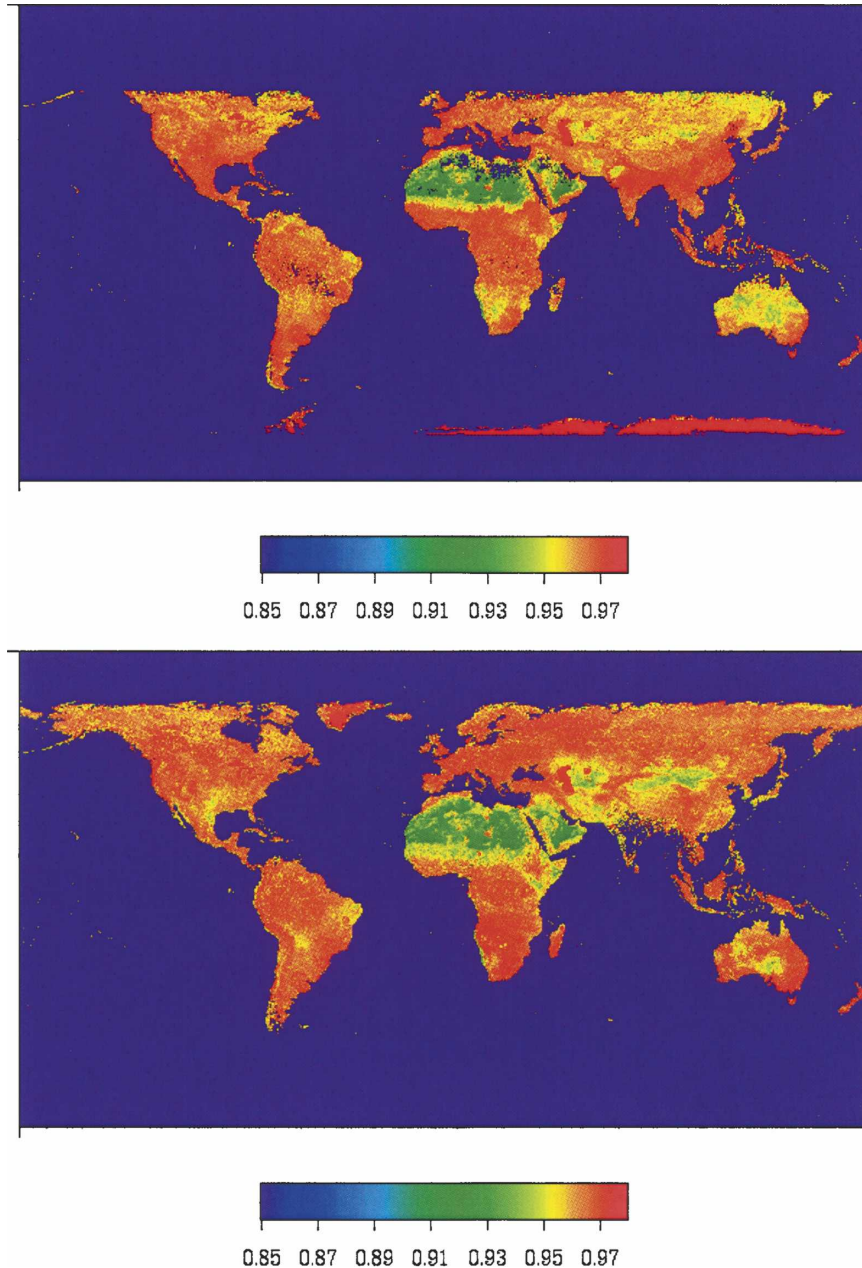
FIG. 3. (a) MODIS broadband emissivity for January 2003. The broadband emissivities are derived from the MODIS spectral band emissivities using a regression equation–based MODTRAN simulation. The resolution of original MODIS emissivity data is 1 km and here is averaged to the T42 resolution of the climate model. (b) Same as in (a), but for July 2001.

tion in the 8–8.7-μm spectral range, where emissivities of soils and minerals may vary significantly. As a conclusion, we recommend Eq. (10) as a more standard conversion approach.

In general, uncertainty of spectral band emissivity is 0.001–0.005 for each band (Wan and Li 1997). Such uncertainty will likely propagate into the final broad-band emissivity value. In addition, uncertainty exists using the regression equation to convert the spectral band to broadband. Figure 4 is the comparison of three-band-converted ε (MODIS bands 29, 31, and 32) and radiative transfer model–simulated broadband emissivity. Our assessment shows that such uncertainty is about ±0.005.
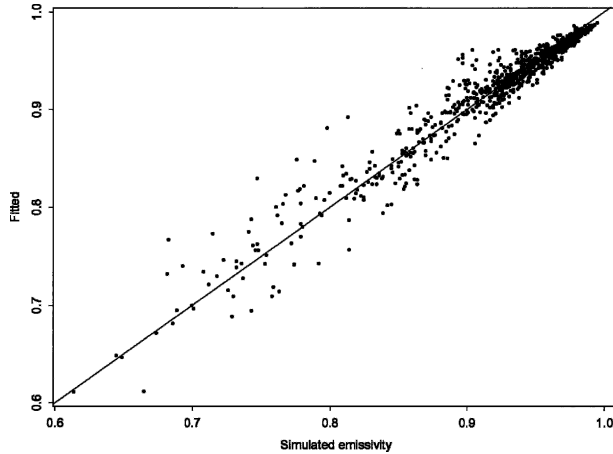
FIG. 4. Examination of three-band-calculated broadband emissivity vs MODIS seven-band-calculated broadband emissivity.

3. Data and model

Monthly mean MODIS observations are used to examine the geographical distributions of ε. The emissivity values in version 4 of the MODIS land surface temperature/emissivity product (MOD11B1) at 5-km sinusoidal grids were obtained from the MODIS Science Team for August 2000 and January 2003. Although being one of the best available data, MODIS emissivity measurements suffer from certain error sources, such as snow surface, clouds cover, or over anonymous high water vapor regions. In this work, we also use the corresponding MODIS land-cover and LAI to demonstrate the dependence of emissivity ε on surface types.

CLM2 is the recently released community land surface model for coupling with NCAR's CAM model (Bonan et al. 2002). CLM2, a model developed by multiple agencies in a communal effort, is based on previous land surface models, such as the Biosphere–Atmosphere Transfer Scheme (BATS; Dickinson et al. 1993), with improved parameterizations for surface snow and hydrology, interception, surface 2-m air temperature, and boundary conditions. We used CLM2 in an offline mode to represent various physical processes among atmospheric–land–ocean applications over the globe. In addition, we performed offline CLM2 simulations over Tucson, Arizona, to examine the skin temperature and sensible and latent heat fluxes with the standard bare-soil parameterization of emissivity (0.96) and with average MODIS-observed bare-soil emissivity ($\sim$0.90). Furthermore, we used the coupled CAM2–CLM2 to examine the emissivity impact in a coupled climate system. Although the absolute values of simulated downward and upward longwave radiation are questionable, partly due to the problematic cloud pa-

rameterization in the GCM, the net longwave radiation is much more reliable.

4. Results

a. Satellite-observed emissivity

Figure 3 compares the geographic distribution of ε in January 2003 and July 2001. In both seasons, Sahara Desert have meaningfully lower ε, with most in ranges of 0.88–0.92. In addition, seasonal variations are evident. For example, in the Saharan deserts, ε can be as low as 0.90 in January and to 0.93 in July, with several pixels having extreme low values of 0.75 (nevertheless, this low values might be retrieval uncertainty; Z. Wan
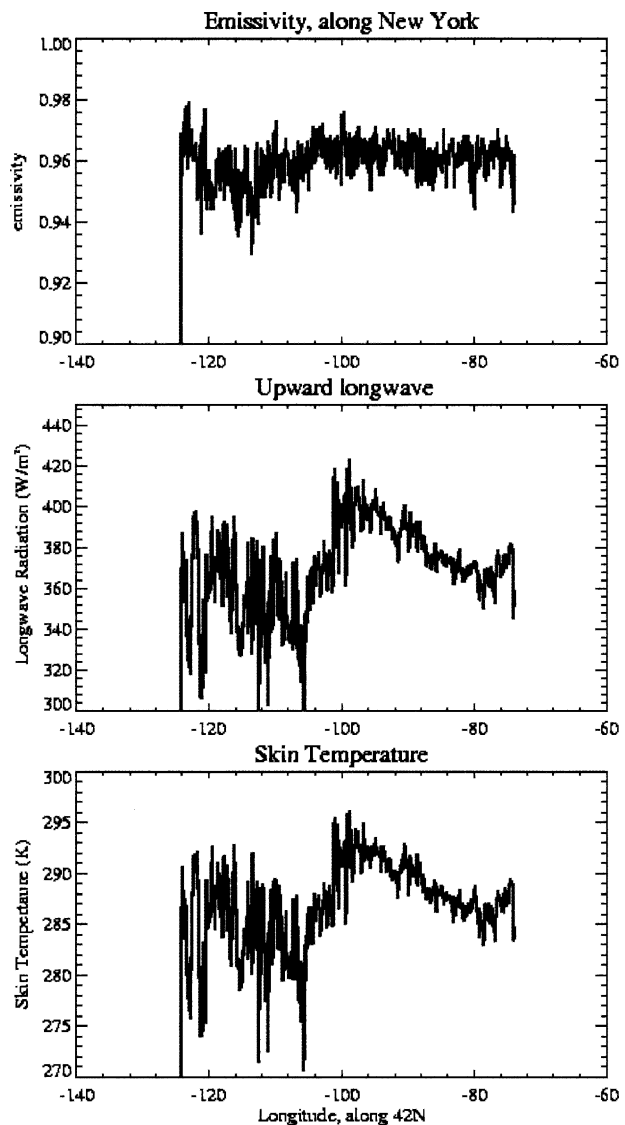

FIG. 5. Emissivity, upward longwave radiation, and skin temperature for 42°N. Data are from MODIS observations. Spatial data resolution is 5 km.
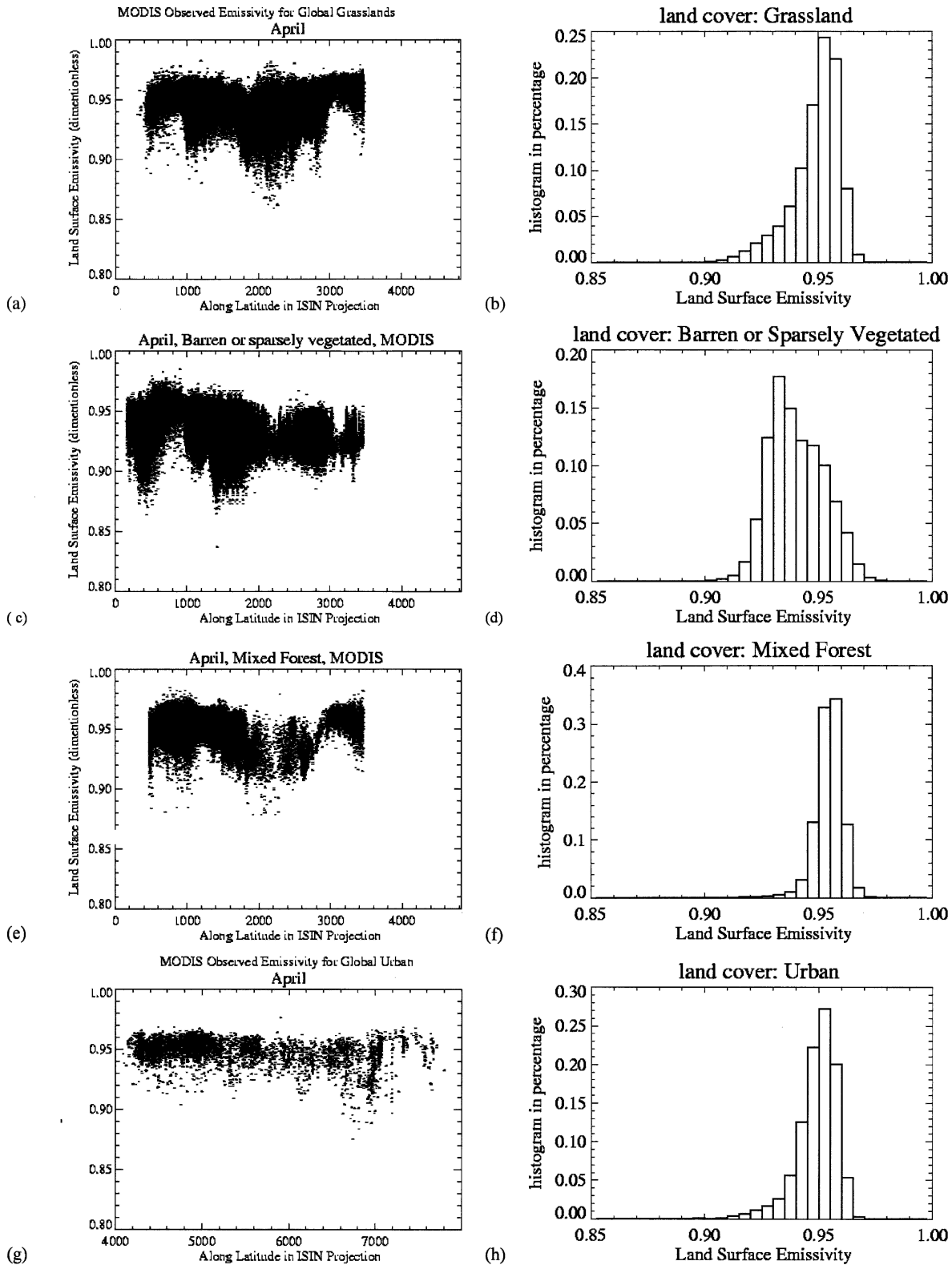
FIG. 6. (a) All grassland pixels over the globe from MODIS. The emissivity values are from MOD11B1 at 5-km sinusoidal grids. The x direction is latitude but in ISIN projection (i.e., 0 is 90°N, 4380 is 90°S, 2190 is 0°). (b) The corresponding histogram in percentage for grassland based on the data in (a). (c) Barren and sparsely vegetated areas, namely, MODIS land-cover type 16. (d) The histogram based on (c). (e) Mixed forest (MODIS land-cover type 5). (f) The histogram based on (e). (g) Urban areas. (h) The histogram based on (g).

2004, personal communication). This may result from the changes of surface wetness or vegetation conditions. Most rainfall in the Sahara occurs from December to March, so in January the soil is relatively wet compared to June–August. In January, low ε (0.94–0.96) occurs over Eurasia high latitudes, due to the low LAI over forests there. Australia also shows low ε, about 0.90–0.96 all year. The dependence of ε on LAI vegetation density and species is also evident. For the boreal forest, the ε ranges from 0.92 to 0.97 between spring and autumn (not shown).

Due to some retrieval problems for January and July, winter and summer ε data are not always reliable at this point, but better data will be available in the near future. However, the general understanding based on MODIS is that, for vegetated areas, winter has a lower ε than summer due to the growth of vegetation as bare soils have lower ε than vegetation.

Figure 5 shows the ε, skin temperature, and upward longwave radiation along the latitude of New York (~42°N) across North America for July 2001. Emissivity does not depend on the object's temperature but varies with the surface land cover. Closely similar shapes are observed on upward longwave radiation and skin temperature, implying that, over midlatitude vegetation areas, the skin temperature plays a more significant role in flux and radiation calculation than that of ε. This is easy to understand since according to the Stefan–Boltzmann law, upward longwave radiation depends on skin temperature raised to the power of 4.

Figure 6 shows ε for different land covers and the corresponding histogram. Significant variations, ranging from 0.87 to 0.97 are observed for bare soil (Fig. 6c), with a peak of about 17% at 0.93 and 12% at 0.95 (Fig. 6d). Such large variations are partly due to the underlying soil conditions and partly due to the growing state of sparse vegetation. Interestingly, the minimum ε is observed at midlatitude Northern Hemisphere desert areas (30°N), with values of 0.86. For comparison, the range of ε for mixed forest (Fig. 6e) is much more moderate than that of bare soil, with the maximum ε as 0.98 and the lower limit as 0.93. Its histogram (Fig. 6f) has evident peaks at 0.95 and 0.96 above 60% and small percentage at other values. Higher and lower values are observed, but rarely, and are considered to be contamination from other surface types. Similar ranges are observed on grasslands (Figs. 6a,b). This agrees with the current understanding that ε varies little over vegetated areas. Figures 6g,h are for urban areas. Due to the much smaller portion of city numbers over the globe, the city has ε ranging from 0.90 to 0.96, regardless of some extreme changes above or below this range. The peak percentage of the city is at 0.945–0.955.
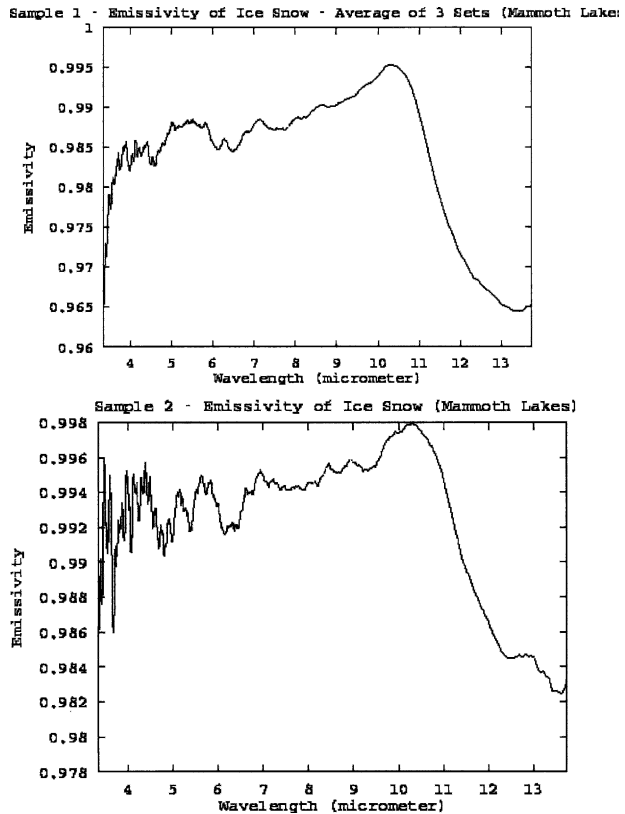

FIG. 7. Samples of snow spectral emissivity. Data are copied from Wan's 2002 emissivity laboratory dataset with permission.

Figure 7 shows two samples for snow spectral ε. Snow ε varies with snow surface roughness, snow water content, and snow particle size. An overall value of 0.99 is observed for infrared wavelength, suggesting that the broadband ε is close to 0.99.

Canopy ε is more uniform than soil ε. Figure 8 shows the LAI and ε relationship over the mideastern United States (27°–55°N, 57°–115°E), as shown in the map (Fig. 8a). The data are for July, from MODIS observations. In this month, LAI over the selected regions varied from 0 to 6. Emissivity varied from 0.92 to 0.98. The mean ε for each LAI is about 0.96 (Fig. 8b). Standard deviation in Fig. 8c represents the spread of ε. A noteworthy observation is that, for almost all LAI values, the standard deviations are as low as 0.005–0.01.

The ε of a natural surface is function of vegetation density and structure, which can be partly represented in LAI. Figure 9 shows the variations of LAI for 40°S–40°N, along 20°E. There is a rough relation observed: the lowest LAI corresponds to the lowest values of ε. A decrease in LAI from 5° to 16°N corresponds to a decrease in ε from 0.97 to 0.92. The lowest values of ε occur in 15°–30°N desert regions, where LAI is not defined—the vegetation barely exists. The correlation
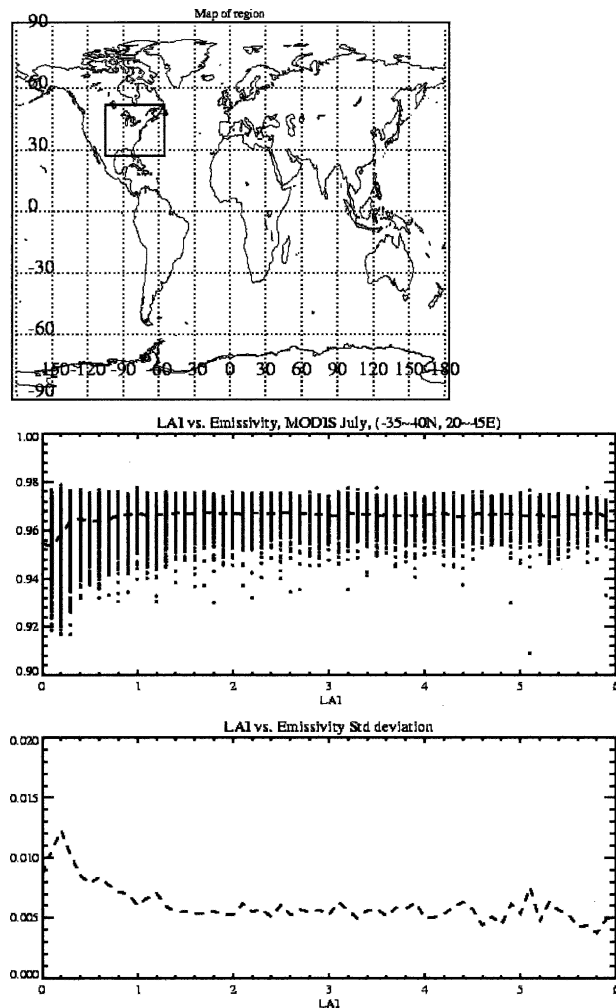
FIG. 8. The relationship between LAI and emissivity. (top) A map of the study regions. (middle) The LAI vs emissivity. The dashed line represents the average value of ε for each LAI value. (bottom) The standard deviation of emissivity for each LAI value.

coefficient between LAI and ε is 0.67. It appears that that the region from 35° to about 17°S is barren, yet it seems to have a high emissivity (0.955–0.972), this is because that vegetation there is small in LAI but it still has shrub structure. Furthermore, the region from 17° to 8°S has small LAI values similar to those for 10°–16°N, but emissivities are quite different for the two regions. This may be because the structure of vegetation is different, and LAI is not the best variable to represent the vegetation structure.

b. Emissivity impacts on land surface modeling

1) SENSITIVITY RESULTS FROM THE OFFLINE LAND SURFACE MODEL

For snow-free grids, CLM2 has bare soil and canopy emissivities. Since canopy emissivity does not vary much, we focus on examining the impacts of soil emissivity using offline CLM2. The control run uses default ε (0.96 for bare soil, 0.97 for vegetation; note in these experiments, we set 0.97 for vegetation-covered regions). The sensitivity run uses MODIS-observed typical emissivity 0.90[3] for bare soil. Figure 10 is the global map of the ground temperature difference between the control run and the sensitivity run for one day in January. Changes are most significant over desert areas, consistent with our previous theoretical analysis. In general, with soil emissivity set as 0.90, the modeled ground temperature increases to about 0.5°–1°C with the maxima increase at the Sahara and its nearby regions. Meanwhile, the difference of 2-m surface air temperature exhibits changes similar to those noticed over desert areas but with relatively small changes in magnitude, due to the delay of atmosphere response to surface energy input (not shown).

Figure 11 is the difference of SH (i.e., the sensitivity run minus the control run). Again, similar changes are noticed over desert areas with flux increases up to 5 W m^{-2} for Saharan regions, due to the increase of ground temperature. Many other regions over the globe have opposite change, namely, a decrease in SH. Figure 12 shows the changes in net LW. Again, the largest changes are observed over the Sahara Desert region, with 1–5 W m^{-2}. Other regions such as Australia, the southwestern United States, the southern part of Africa, and eastern Asia around 50°N, 120°E have similar changes. Although the magnitude of SH and LW change are relatively small ($<$5 W m^{-2}), it is daily mean and instantaneous value can be much higher. Therefore, we need to examine the diurnal variations and seasonality of this error. More importantly, we need to examine the error in a real surface–atmosphere climate system using a coupled GCM.

Since the largest impacts of ε are over desert areas, we conducted further model sensitivity studies over one of these areas: Tucson, Arizona ($\sim$30°N, 112°W). The atmospheric input is based on observations. The control run uses the default emissivity of CLM (0.96), and the sensitivity run keeps everything the same as the control run except for setting soil emissivity as 0.90, which is the observed typical value for soil there. The runs start at Julian day 132 (in 1993) with output every 20 min and averaged to daily mean (as presented here). The comparison shows that skin temperature with $\varepsilon =$ 0.90 is lower than that of $\varepsilon =$ 0.96, with the difference

---

[3] We also conducted sensitivity runs by setting soil emissivity as 0.86, 0.92, and 0.94. The patterns of the impact are similar as presented here, with the magnitude differing a little.
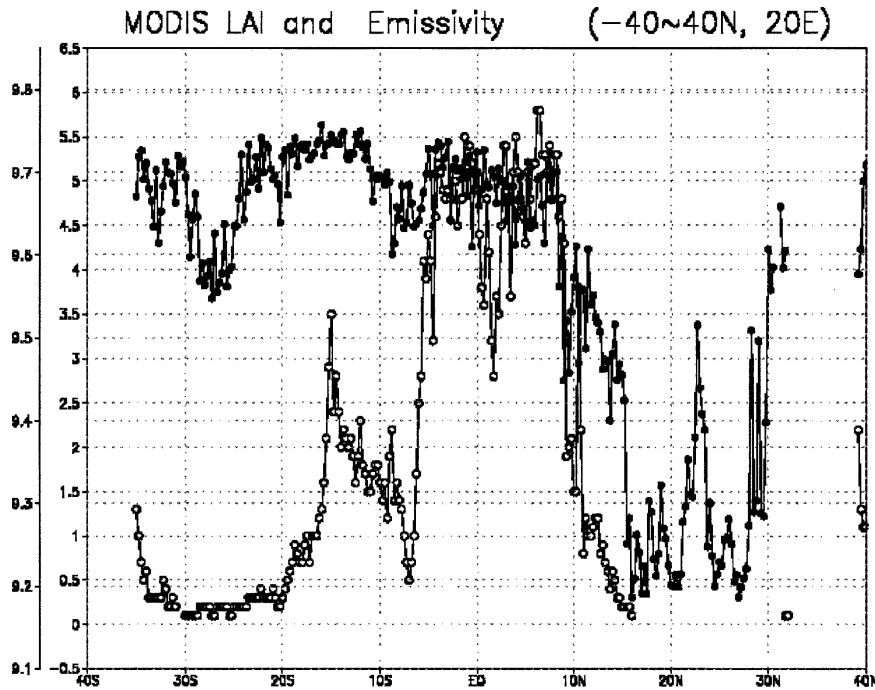
FIG. 9. LAI and emissivity relationship for 40°N–40°S, and 20°E. The open circle is LAI and the dotted line is for emissivity. The scale of emissivity is multiplied by 10.

in general as −4°C (Fig. 13a). During some daytime periods, the difference can be as high as 10 K (as can be seen from the 20-min output). At nighttime, the difference is little. Similarly, sensible and latent heat flux changes between control and sensitivity runs are also very large, 10 W m^{-2} to as high as 50 W m^{-2} (Figs. 13b,c). Furthermore, the changes of latent heat flux can be negative. It seems that the impact of ε on sensible
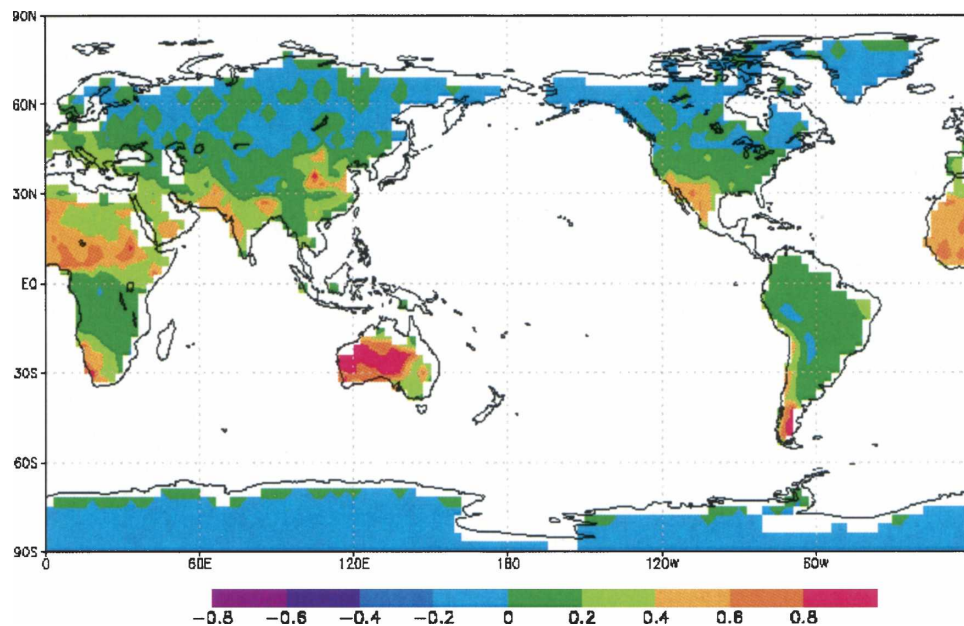
FIG. 10. Offline CLM-simulated ε impact on the ground temperature (K) sensitivity run ($\varepsilon = 0.90$) minus the control run ($\varepsilon = 0.96$ as the default). The data are daily averages of January 1998.
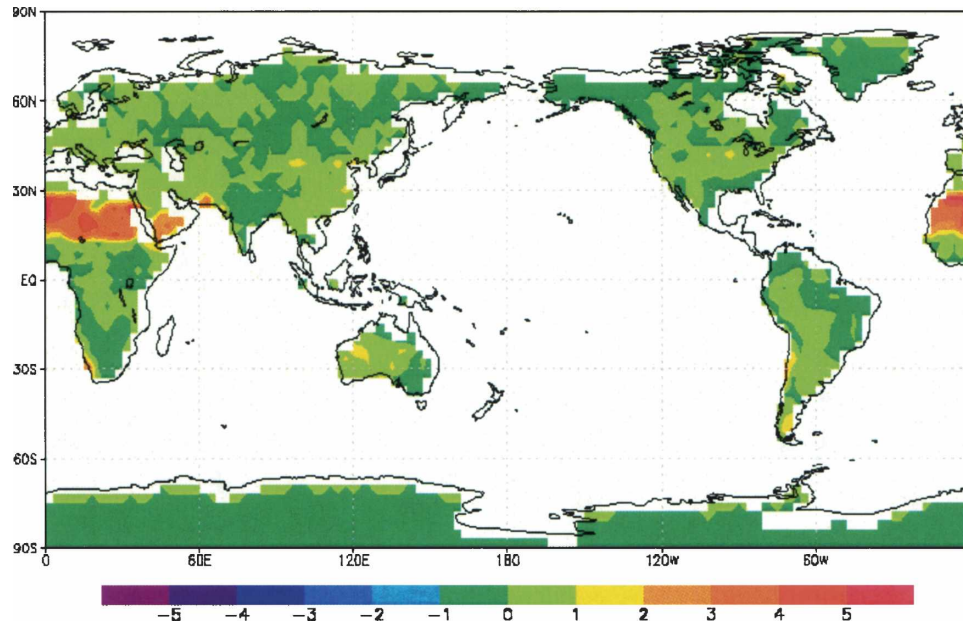
FIG. 11. Same as in Fig. 10, but for sensible heat flux (W m^{-2}).

heat flux is larger than it is on latent heat flux since the soil moisture there is very limited.

The Tucson study (Fig. 13) is more reliable as the atmosphere forcing data in this case are the real observations, and thus the magnitude and sign were reliable. By contrast, in the offline CLM sensitivity study (Fig. 10), the atmosphere forcing was from the NCEP re-

analysis, which has reported problems in their surface wind and surface air temperature (K. Trenberth 2002, personal communication). Another evidence is that Fig. 14 from the coupled CAM2–CLM2 also shows that current high constant emissivity induces warm bias at the surface, which is consistent with Fig. 13 but not with Fig. 10. Nevertheless, we still need to keep offline CLM
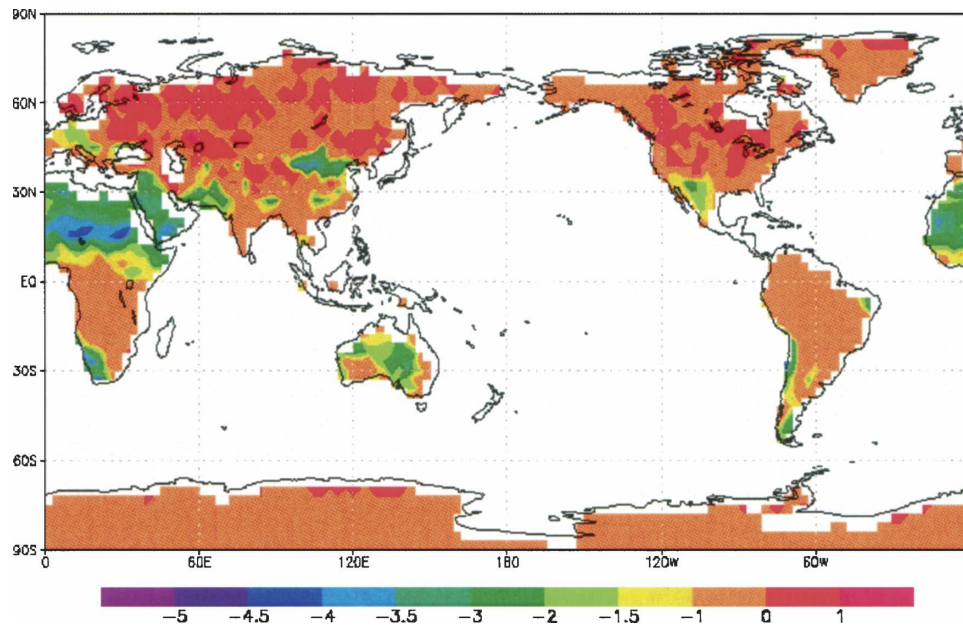

FIG. 12. Same as in Fig. 10, but for net longwave radiation (W m^{-2}).
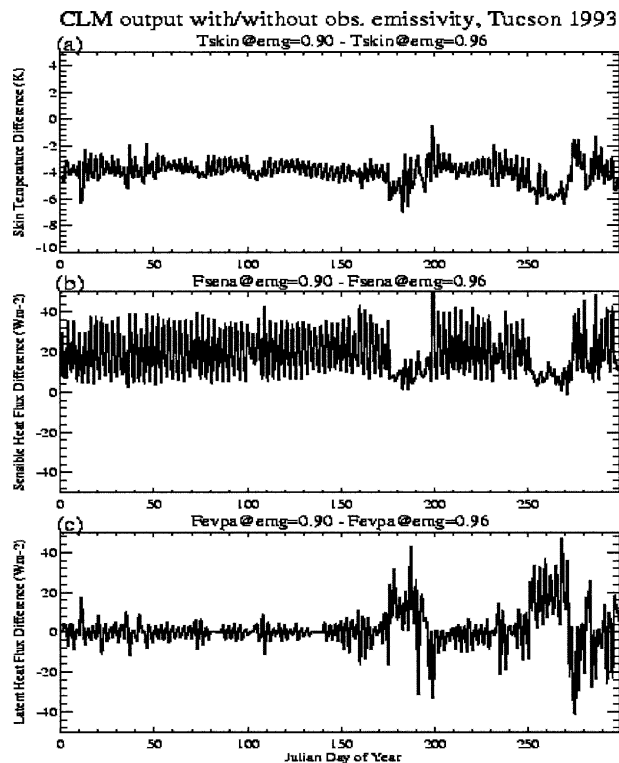
FIG. 13. Offline CLM simulations for Tucson, AZ, in 1993. Presented are differences between the run with emissivity settled as the observed value (0.90) and the run with the default emissivity (0.96): (a) skin temperature, (b) sensible heat flux, and (c) latent heat flux from surface to air.

study here to show that the land model by itself is sensitive to the emissivity.

2) RESULTS FROM A COUPLED GCM

In a coupled climate system, the uncertainties and impacts of ε may propagate into the atmosphere and the atmospheric noise may enhance or reduce ε's impact on the surface. Therefore, it is interesting to study the effects of ε in the land–atmosphere climate system using the GCM. We conduct a series of sensitivity runs using NCAR CAM2–CLM2. To avoid spinup, we use the NCAR specifically recommended initial condition and boundary condition files for the land surface model. Similar to offline runs, the control run sets ε as default values, and the sensitivity run sets the soil emissivity at 0.90, and canopy emissivity at 0.97. Both the control and sensitivity cases run the model for a short time. Running the model for a short time is based on two considerations: first, since in the two runs only ε is changed and any other condition is the same, the differences between the two runs are caused by the ε impacts; second, we noticed that after a long running time, the model output became quite noisy. This may be due to the atmosphere model's noise being transported into model outputs (R. E. Dickinson 2003, personal communication).

Figures 14a,b show the global distribution of simulated surface air temperature. The model gives reasonable simulation for this variable. Figures 14c,d show the ε impacts evident over the desert and semidesert regions. A decrease of ε causes a decrease of surface air temperature. Namely, current high constant ε results in warm bias over desert regions on the surface air temperature field, which can be as high as 1.5°C over Saharan regions. By comparison, the emissivity (ε) impact on skin temperature seems to be smaller than its impact on the surface air temperature. Figure 15 shows skin temperature decreases as much as 1°–1.5°C over certain desert regions of the southwest United States, Eurasia, Australia, and the Sahara. The warming bias at surface skin and air levels imply an enhanced sensible heat flux from the surface to air. Nevertheless, we notice that over certain small regions, the ε impacts are opposite to the rest of the land regions, such as 0°, 20°E, where the control case has lower air temperature than the sensitivity case, resulting in a negative value in Fig. 15a. Nevertheless, such negative values are less significant on Fig. 15b, implying that ε impacts on this region are relatively weak, so that the signs of the impact do not always remain evident.

5. Uncertainties and discussion

Broadband emissivities have uncertainties stemmed from MODIS spectral emissivity ε_λ as well as the conversion equation used to calculate broadband ε from ε_λ. As previously reported, over certain areas of South America and tropical Africa, cloud cover results in missing ε. It is also questionable over certain Saharan areas, where evident ε changes (3%–5%) from January to July occur. Whether such large changes are due to the seasonality of soil wetness or due to retrieval problems is unknown. Nevertheless, in general, MODIS ε shows encouraging accuracy in terms of geographic distribution and interannual variations (Z. Wan 2003, personal communication). In addition, the regression equations used to convert MODIS ε_λ into broadband ε only give a statistical average for ε. However, our research shows that uncertainty induced by the regression approach is less than 1%.

From a land surface modeling perspective, the importance of ε has been ignored so far. Compared with surface albedo, which determines the net surface solar
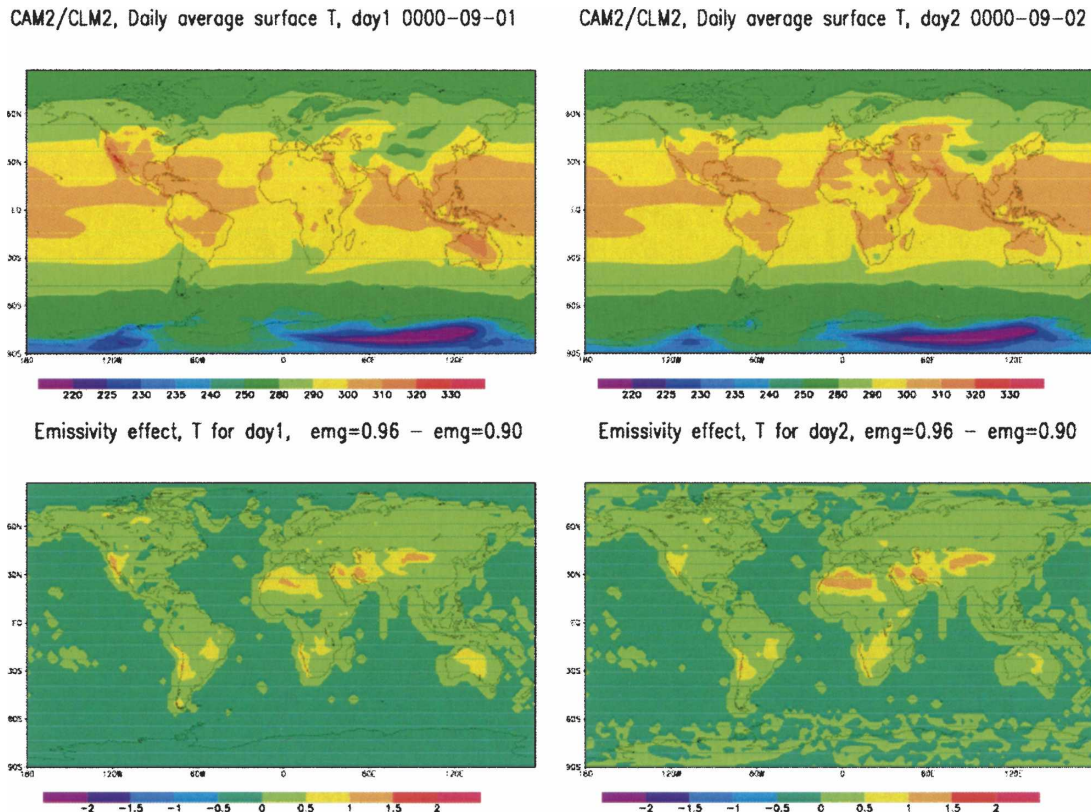
FIG. 14. Emissivity impacts in the coupled model CAM2–CLM2: (a) control run of 1-day daily averaged surface air temperature; (b) control run of another daily averaged surface air temperature; (c) emissivity impact on surface air temperature, the control run minus the sensitivity run; (d) same as in (c) but for another day.

radiation, ε may be less critical in the surface energy budget. But it is very important over arid and semiarid areas and at least should be taken into account there. By changing net longwave radiation from that which was supposed to be from blackbody, ε affects skin temperature, sensible, and latent heat flux simulations. MODIS global ε observations show great value for use in land surface models.

Optimally, use of MODIS observations, or other remotely sensed ε information such as those from the ASTER in land surface models is a continuing task. Two approaches are practical: one is to use a lookup table to show ε variations as a function of the soil condition, season, and land cover, and then to parameterize ε in the model; another is to directly use MODIS ε observations into the model to replace current prescribed, unrealistic values. Unfortunately, scaling up ε observations from MODIS fine resolution into the model grid cell requires more research. Because it is difficult to accurately measure ε, and because ε over some biologically distinct cover types are nearly the same, it may be adequate to use single values for each discrete land-cover type to represent ε in a GCM rather than directly input satellite global or regional observations into a model.

Inconsistencies exist in placing satellite-based ε into a land surface model. One is that satellites can only measure spectral band ε_λ; therefore, satellite data need to be converted into broadband. We recommend a regression equation approach in this paper. Another inconsistency is that over partially vegetation-covered regions, the satellite-measured ε, even at a resolution as fine as 1 km, is a combination of soil and vegetation emissivities. How to interpret this combined information into a model's canopy and ground ε is a question that needs to be addressed.

The ε impacts presented here are from one model. It is valuable to reevaluate these impacts using other models and to examine to what extent these impacts are valid. Before a model can be used to examine ε impacts, however, the formulations of land surface needs to be carefully checked, since some models derive the land formulations by setting ε as a unit for simplification and ignore certain terms as discussed in Deardoff (1978).

Emissivity effect, T for day1, emg=0.96 – emg=T42

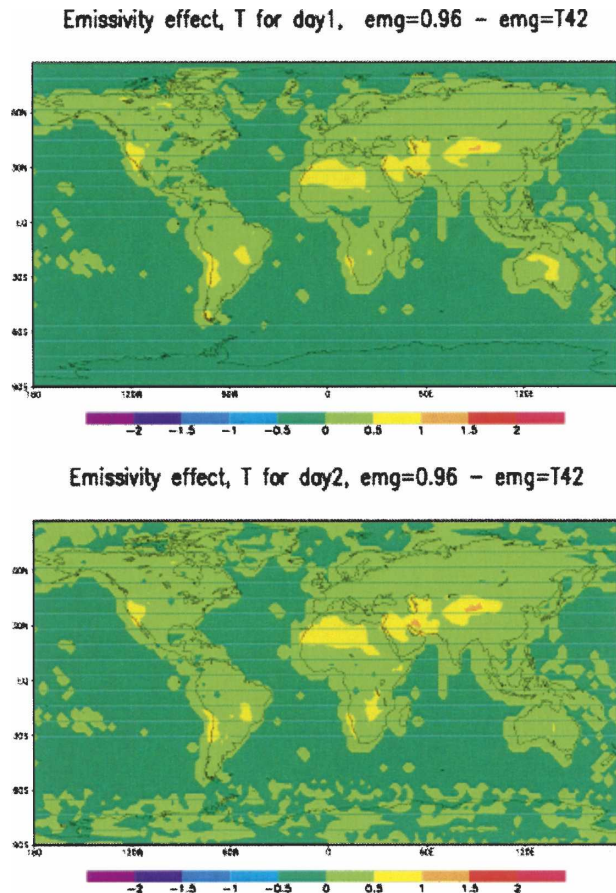## Emissivity effect, T for day2, emg=0.96 – emg=T42

FIG. 15. Coupled CAM2–CLM2 simulated emissivity impact on surface temperature (K) for two random days in September. The difference is the control run minus the sensitivity run. The control run uses CLM default soil emissivity ($\varepsilon = 0.96$), and sensitivity run uses satellite-observed emissivity at T42 resolution.

Such neglect will cause the ε to have a misleading effect.

REFERENCES

Bonan, G. B., K. W. Oleson, M. Vertenstein, S. Levis, X. Zeng, Y. Dai, R. E. Dickinson, and Z. Yang, 2002: The land surface climatology of the community land model coupled to the NCAR community climate model. *J. Climate,* **15,** 3123–3149.

Deardorff, J. W., 1978: Efficient prediction of ground surface temperature and moisture with inclusion of a layer of vegetation. *J. Geophys. Res.,* **83** (C4), 1889–1903.

Dickinson, R. E., A. Henderson-Sellers, P. J. Kennedy, and M. F. Wilson, 1986: Biosphere-Atmosphere Transfer Scheme (BATS) for the NCAR community climate model. NCAR Tech. Note TN-275+STR, NCAR, Boulder, CO, 48 pp.

——, ——, and ——, 1993: Biosphere-Atmosphere Transfer Scheme (BATS) Version 1E as Coupled to the NCAR Community Climate Model. NCAR Tech. Note NCAR/TN-387+STR, NCAR, Boulder, CO, 72 pp.

Francois, C., C. Ottle, and L. Prevot, 1997: Analytical parameterization of canopy directional emissivity and directional radiance in the thermal infrared. Application on the retrieval of soil and foliage temperatures using two directional measurements. *Int. J. Remote Sens.,* **18,** 2587–2621.

Fuchs, M., and C. B. Tanner, 1966: Infrared thermometry of vegetation. *Agron. J.,* **58,** 597–601.

Idso, S. B., R. D. Jackson, W. L. Ehrler, and S. T. Mitchell, 1969: A method for determination of infrared emittance of leaves. *Ecology,* **50,** 899–902.

Jin, M., R. E. Dickinson, and A. M. Vogelmann, 1997: A comparison of CCM2/BATS skin temperature and surface-air temperature with satellite and surface observations. *J. Climate,* **10,** 1505–1524.

Liang, S., 2001: An optimization algorithm for separating land surface temperature and emissivity from multispectral thermal infrared imagery. *IEEE Trans. Geosci. Remote Sens.,* **39,** 264–274.

——, 2004: *Quantitative Remote Sensing of Land Surfaces.* John Wiley and Sons, 534 pp.

Logan, L. M., G. R. Hunt, and J. W. Salisbury, 1974: The use of mid-infrared spectroscopy in remote sensing of space targets. *Infrared and Raman Spectroscopy of Lunar and Terrestrial Materials,* C. Karr, Ed., Academic Press.

Nerry, F., J. Labed, and M. P. Stoll, 1990: Spectral properties of land surfaces in the thermal infrared. 1. Laboratory measurements of absolute spectral emissivity signatures. *J. Geophys. Res.,* **95,** 7027–7044.

Prabhakara, C., and G. Dalu, 1976: Remote sensing of the surface emissivity at 9μm over the globe. *J. Geophys. Res.,* **81,** 3719–3724.

Rowntree, P. R., 1991: Atmospheric parameterization schemes for evaporation over land: Basic concepts and climate modeling aspects. *Land Surface Evaporation Measurement and Parameterization,* T. J. Schmugge and J. Andre, Eds., Springer-Verlag.

Sellers, P. J., Y. Mintz, Y. C. Sud, and A. Dalcher, 1986: A simple biosphere model (SiB) for use within general circulation models. *J. Atmos. Sci.,* **43,** 505–531.

Snyder, W. C., Z. Wan, Y. Zhang, and Y.-Z. Feng, 1998: Classification-based emissivity for land surface temperature measurement from space. *Int. J. Remote Sens.,* **19,** 2753–2774.

Van De Griend, A. A., and M. Owe, 1993: On the relationship between thermal emissivity and the normalized difference vegetation index for nature surfaces. *Int. J. Remote Sens.,* **14,** 1119–1131.

Wan, Z., and Z. Li, 1997: A physics-based algorithm for retrieving land-surface emissivity and temperature from EOS/MODIS data. *IEEE Trans. Geosci. Remote Sens.,* **35,** 980–996.